Improving PVDF Hollow Fiber Membranes for CO_2 Gas Capture

Yaocihuatl Medina-Gonzalez,[1,2†] Elsa Lasseuguette,[1,2] Jean-Christophe Rouch,[1,2] and Jean-Christophe Remigy[1,2]

[1]*Université de Toulouse, INPT, UPS, Laboratoire de Génie Chimique, Toulouse cedex, France*
[2]*CNRS, Laboratoire de Génie Chimique, Toulouse cedex, France*

Poly(vinylidene fluoride) (PVDF) hollow fiber membranes were obtained by the phase inversion technique. The influence of internal coagulant viscosity (0.001 to 3 Pa s) and air gap (0.6 to 86.4 cm) on the structure and mechanical resistance of the fibers was studied. A "sponge-like" structure free of macrovoids was obtained by using polyvinyl alcohol (PVA) with N-methyl pyrrolidinone and water as internal coagulant (viscosity 3 Pa s). The effect of the air-gap was studied in order to control the structure and obtain mechanically resistant membranes with tensile strength at break between 2.2 and 54.3 N/mm^2 and pure water permeability ranging from 4 to 199 Lh^{-1}m^{-2}bar^{-1}. CO_2 permeability of these membranes was measured and found to be in the range of 365 to 53200 NLh^{-1}m^{-2} bar^{-1}. The "Dusty Gas" model (DGM) was used to calculate the pore size of the membranes from CO_2 permeability experiments, obtaining pore radius values going from 0.6 to 10.8 µm. Results from modeling were compared with pore sizes observed in SEM images showing that this model can accurately predict pore radius of sponge-like structures; however, pore sizes of membranes presenting sponge-like structures together with finger-like pores were inaccurately predicted by the DGM.

Keywords CO_2 capture; contactors; dusty gas model; polyvinyl alcohol; porous membranes; PVDF

1. INTRODUCTION

In recent years, the abatement of greenhouse gases has become a major concern in industrial and chemical engineering. Amongst the principal sources of CO_2, are stationary ones where CO_2 can be captured directly. Several technologies have been proposed to capture CO_2 from stationary sources, including absorption, adsorption, cryogenic distillation, and membrane separation (1a). Traditionally, packed columns have been used for absorption but this technique suffers from various problems including flooding, channeling, entrainment, and foaming (1b) Membrane separation presents many advantages, like simplicity, compactness, and easy integration in already installed facilities (2,3). Contactors are promising alternatives to packed columns. In a contactor, a microporous membrane separates the gas and liquid phases. Gas diffuses through the membrane and comes into contact with an absorption liquid. Absorption can be performed either physically or chemically. This system eliminates the operational problems present in packed columns. In terms of energy requirements, membrane contactors compete with absorption when the CO_2 content in the feed exceeds 20%, which corresponds to a large number of industrial situations (4). Other advantages of contactors are the large surface of the membrane modules, their low weight, and easy scale-up. Removal of CO_2 from gas streams by a membrane contactor has been a focus of research since the 1980s. To improve CO_2 removal, several factors need to be considered: membrane materials and properties, absorption solutions, and modules. As membrane properties such as selectivity and permeability are key elements that dramatically influence permeate purity, CO_2 recovery rate and the energy consumed during CO_2 capture, research in these fields is key to achieving good greenhouse gas recovery.

Hollow fibers provide a high contacting surface area per unit volume and they have been commercialized for gas absorption/stripping (5). However, one of the drawbacks of these arrangements is the additional mass-transfer resistance added by the membrane, especially if the membranes are wetted by the absorption solution. The porous hydrophobic polypropylene hollow fibers that are currently used in gas/liquid contactors appear to undergo wetting with time when they are used with volatile amines (6) or other common CO_2 absorption liquids (7).

Polyvinylidene fluoride (PVDF) is a semi-crystalline polymer with excellent chemical and thermal resistance (8,9). Its highly hydrophobic character allows its utilization in membranes for gas absorption, oil/water

†Actual address for Y. Medina Gonzales Laboratoire de Génie Chimique, Campus INP-ENSIACET, 4 allée Emile Monso, 31030 Toulouse cedex 4.

Address correspondence to Yaocihuatl Medina-Gonzalez, Laboratoire de Génie Chimique, 118 route de Narbonne, Toulouse 31062, France. Tel.: +33 (0)5 34 32 37 02; Fax: +33 (0)5 34 32 36 97. E-mail: Yaocihuatl.MedinaGonzalez@ensiacet.fr

separation, membrane distillation, and microfiltration (10, 11). Such membranes are already commercially available from MBR, Memstar Technology, among other companies. Especially in gas absorption using a gas/liquid membrane contactor, hollow fiber membranes are required to stay dry during long periods even during liquid contact. In these cases, hydrophobicity is a very important factor to be considered (7,12). PVDF hollow fibers can be prepared by a phase inversion technique leading to liquid-liquid demixing that typically produces a porous structure. In a membrane with these characteristics, the porous substrate provides mechanical support without decreasing mass transfer. However, considerable mass-transfer resistances can arise from the development of skin layers (13, 14). Hollow fiber membranes with inner skinless structures present low mass-transfer resistance and high permeability. A phenomenon appearing when crystallizable polymers such as PVDF are used is solid-liquid demixing occurring in the crystallizable fragments of the polymer, to form membranes consisting of interlinked crystalline particles (leafy morphology) (15).

Several groups have successfully achieved the fabrication of PVDF microporous membranes in the past (16, 17). Nevertheless, when PVDF membranes with pore sizes of less than 100 nm need to be produced, permeability undergoes a huge decrease and macrovoids appear, resulting in fragile structures not suitable for high-pressure applications. One way to achieve higher permeability and control pore sizes is to change the activity of the internal coagulant (water) by using mixtures of water/NMP. However, some studies have shown that the use of these mixtures results in non-circular hollow fibers (18) with non-uniform wall thickness. These non-uniformities lead to fragile points inside the structures, resulting in easily collapsing membranes.

The objective of this work was to prepare and characterize PVDF hollow fibers having a sponge-like structure and circular shape by using the phase inversion technique. Polyvinyl alcohol (PVA) was used to increase the viscosity of the internal coagulant (water) and to decrease its activity. PVA presents multiple hydroxyl groups, which provide this polymer with good water solubility. However, these hydroxyl groups can produce many very strong hydrogen bonds between both intra-PVA and inter-PVA macromolecular chains, conferring high viscosity on its water solutions. PVA is also a semicrystalline polymer, and its dissolution process includes two stages: swelling and dissolution. During the first stage, water enters the amorphous region of PVA then, during a second step, the crystalline region, until the PVA is completely dissolved (19). The strong capacity of PVA for hydrogen-bonding leads to a highly viscous solution in water and sometimes leads to gel formation at low PVA concentrations, depending on its degree of polymerization and hydrolysis. In this study, incorporation of PVA in the bore solution allowed the formation of circular hollow fibers by limiting the movement of the interface between the polymer solution and the internal coagulant. Characterization of hollow fibers included water and CO_2 permeability, structural characterization from SEM photographs and mechanical properties. Results of modeling pore sizes and porosity-tortuosity factors by using the Dusty Gas Model together with CO_2 permeability results are also reported. This study is a step forward in the understanding and control of the morphology and properties of highly hydrophobic PVDF membranes presenting properties suitable for greenhouse gas separation and absorption when used in a gas/liquid contactor.

EXPERIMENTAL PROCEDURES

Materials

The membrane material PVDF (Kynar 301 F) was purchased from Arkema, France. NMP was purchased from Gaches Chimie, France. Polyvinyl pyrrolidone Mw 8000 Da (PVP K15) was used as porogen and supplied by Sigma-Aldrich. PVA (Mw 124 000–186 000 Da) was obtained from Sigma-Aldrich. All materials were used without further purification.

Hollow Fiber Membrane Fabrication

Hollow fiber (HF) membranes were fabricated by the dry/wet spinning technique using a spinning pilot. The spinneret used is shown in Fig. 1. Four different internal coagulants were tested: water, water/NMP 50/50 w/w, NMP/water/PVA and water/PVA. In the case of PVA solution, the ratio of NMP/Water was kept constant and we added 8% of PVA in order to increase the dope solution viscosity. Dope solution was constituted of PVDF/PVP/NMP 20/6/74 w/w/w; dope solution flow rate was controlled at 5.5 cm^3 min^{-1}. Internal coagulant feed rate and spinning speed were set to 3.3 cm^3 min^{-1} and 5.2 m min^{-1}, respectively. The coagulation bath was filled with tap water at 25°C. Internal coagulant and dope solution temperatures were set to 25°C. After coagulation, the

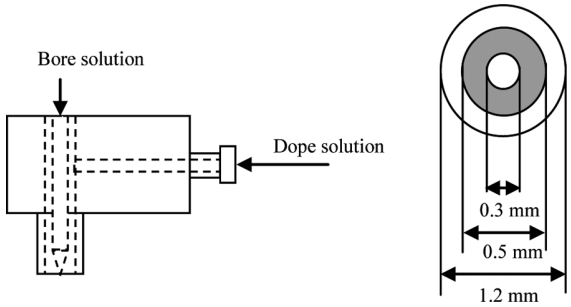

FIG. 1. Spinneret used in this study.

TABLE 1
Spinning conditions used to obtain the hollow fiber membranes. Internal coagulant 1: water, 2: Water/NMP (50%, 50%), 3: Water/NMP/PVA (46%, 46%, 8% respectively) 4: Water/PVA (92%, 8% respectively). PWP = Pure Water Permeability. – means not measured. CO_2 permeability is expressed in $NLh^{-1}m^2\,bar^{-1}$ and in Barrer (barrer in brackets), 1 Barrer = 1×10^{-10} cm^3 gas (STP) cm/cm^2 s cmHg. NL means Normal liter, a liter of gas at standard conditions of pressure and temperature

	Air gap (cm)	Wall thickness (mm)	PWP at 20°C $Lh^{-1}m^{-2}bar^{-1}$	CO_2 permeability $NLh^{-1}m^{-2}bar^{-1}$ (Barrer)	H_2O comp. pressure (bar)	CO_2 comp. pressure (bar)
1a	0.6	0.265	131	32720 (24.6)	2.0	3
1b	18.4	0.353	136	22350 (26.4)	–	–
1c	43.0	0.312	78	53200 (47.1)	2.0	>3.5
1d	86.4	0.282	77	41140 (32.9)	2.0	>5
2a	0.6	0.305	65	26600 (23)	2.4	–
2b	18.4	0.257	32	36200 (26.4)	4.0	–
2c	35.0	0.255	27	42700 (30.9)	3.8	–
2d	78.0	0.225	14	32000 (20.4)	6.0	–
3a	0.6	0.201	5	1200 (0.7)	–	7.7
3b	18.4	0.233	4	720 (0.5)	3.1	–
3c	35.0	0.207	5	–	3.2	–
3d	54.2	0.204	5	365 (0.2)	3.5	–
3e	78.0	0.205	10	6300 (3.7)	2.0	–
4b	18.4	0.219	199	4720 (2.9)	–	11.2
4c	35	0.221	55	4790 (3)	–	5.2
4d	54	0.210	173	2250 (1.3)	1.2	17
4e	78	0.207	100	1200 (0.7)	1.2	7.7

hollow fibers were stored in a water bath at 25°C for 24 hours to remove residual solvent. Different structures were obtained by varying the air gap between the spinneret and the coagulation bath and the composition of the bore fluid.

Table 1 shows the spinning conditions used in our experiments and Table 2 gives the viscosities of the bore liquids measured using an Anton Paar MCR 301 rheometer equipped with a rotational cylinder measuring system.

Hollow Fiber Membrane Characterization

Sem

Scanning Electron Microscopy (SEM) was performed with a JEOL JSM 6700 F or a Hitachi TM-1000. Samples of PVDF hollow fibers were dried overnight at 60°C then cryo-fractured using liquid nitrogen in order to obtain a smooth surface to be observed by the SEM.

TABLE 2
Viscosities of the four bore liquids used

	Bore liquid	Viscosity (Pa s)
1	Water	0.001
2	Water/NMP 50/50	0.005
3	Water/NMP/PVA 46/46/8	3.00
4	Water/PVA 92/8	0.65

Water Permeability

Laboratory-made HF modules were fabricated using the wet hollow fibers obtained. Modules were 1.3 cm in diameter and 25 cm in length. Each module was filled with 6 PVDF fibers. Pure water permeability tests were performed in the equipment shown in Fig. 2a using water purified by reverse osmosis. In a typical experiment, the tank was filled with UHQ water; compressed air was used to pressurize the tank at the desired pressure. Water flow through membranes was measured using a chronometer and a measuring cylinder. Water temperature was recorded for each experiment.

CO_2 Permeability

As we were interested in CO_2 absorption applications using gas liquid contactors, stainless steel modules were fabricated with the membranes produced, previously dried at room temperature for 5 days (water content less than 3 wt% measured with a drying balance). These modules allowed the determination of CO_2 permeability of the membranes using the experimental set-up shown in Fig. 2b. In this equipment, the flow rate of CO_2 through the

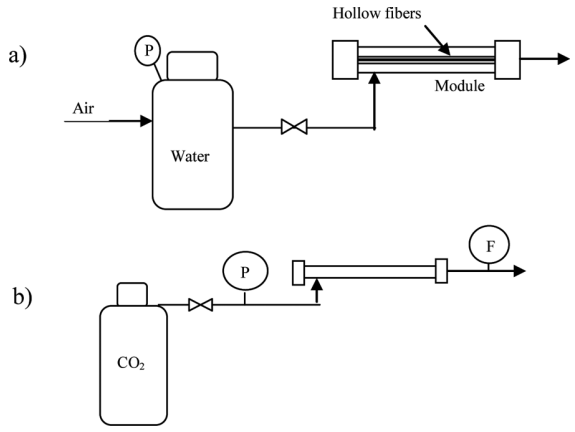

FIG. 2. a) Lab-scale equipment for water permeability measurements, b) Lab-scale equipment used in gas permeability experiments.

membranes was measured at various transmembrane pressures ranging from 0 to 10 bars at room temperature. At these conditions swelling and/or CO_2-induced cristallinity of PVDF are negligible, in all the cases, experiments were conducted during short periods of time to insure CO_2 effect on polymer cristallinity does not affect the measurements (20).

CO_2 permeability has been defined as the volume of CO_2 (at standard conditions) passing through a unit area of membrane per unit time (flux of CO_2 at standard conditions), with a unit pressure difference across the sample. Permeability can take into account the thickness of the membrane according to equation (1), which has been calculated as well.

$$P = \frac{(quantity\ of\ permeant) \times (sample\ thickness)}{(area) \times (time) \times (pressure\ drop\ across\ the\ sample)} \quad (1)$$

Experiments were conducted as follows: CO_2 from the cylinder was passed through the membranes by controlling inlet pressure. Gas flow was measured at the exit by using a flow meter.

Mechanical Properties

In order to obtain information about the mechanical properties of our membranes, tensile strength and elongation at the elastic limit and at break where determined from tension tests performed in a one-column INSTRON, Model 3342. The tests were performed at a fixed speed of 200 mm min^{-1} with an initial sample length of 70 mm. We used a special jaw designed for fiber testing (model T353-2). These experiments were performed on membranes previously dried as described in the previous section. Reproducibility of these results has been assured by performing 10 measurements for each membrane.

Pore Size Determination by using the "Dusty Gas" Model

When the structure-related parameters are linked directly to the permeation-related parameters in a membrane, it is necessary to differentiate between the pore shape and its size. In general, simple model descriptions deviate from the real morphology of membranes, and sometimes these deviations can be very important. Gas permeability can help us to understand the transport mechanisms occurring during gas transport, as Knudsen (free-molecule) and Poiseuille (viscous) flows. The first mechanism is present when the pressure is low, so the mean free path of the gas molecules exceeds the tube diameter. The second is present when the pressure is high, so the mean free path of the molecules is small compared to the diameter of the tube. However, in the transition region, both mechanisms must be considered to reach good approximations. The model called the "Dusty Gas" model (DGM) (21–24) takes both transport mechanisms into account.

In the DGM method, the porous medium is visualized as an array of dust particles held stationary in space. Based on this model, a general flux equation for a gas that permeates through a porous medium in the Knudsen-Poiseuille transition can be obtained by (25–28)

$$N = -\frac{M}{RT}\left[K_0\overline{\nu} + \frac{P_{avg}B_0}{\mu}\right]\frac{\Delta P}{\delta} \quad (2)$$

where

N is the mass flux (kg $m^{-2}s^{-1}$)
R is the universal gas constant (8.314 J mol^{-1} K^{-1})
T is the absolute temperature (K)
M is the molecular weight of the gas (kg mol^{-1})
ΔP is the pressure drop across the membrane (Pa)
μ is the viscosity of the gas (Pa s)
δ is the membrane thickness (m)
v is the mean molecular speed of the gas (m s^{-1})
P_{avg} is the average pressure across the membrane (Pa)
B_0 is a constant that depends on the medium alone. K_0 is related to a geometric constant characteristic of the dust particles. This constant depends on the angular scattering pattern with which the gas molecules rebound from dust particles.

If we assume uniformly straight cylindrical pores, K_0 and B_0 can be obtained in the following way

$$K_0 = \frac{2\varepsilon r}{3\tau} \quad (3)$$

$$B_0 = \frac{\varepsilon r^2}{8\tau} \quad (4)$$

Where

ε is the membrane porosity
τ is the tortuosity factorr is the pore radius.

Equation (1) can be rearranged as follows

$$\frac{NRT\delta}{\Delta PM\overline{\nu}} = K_0 + B_0 \frac{P_{avg}}{\mu\overline{\nu}} \quad (5)$$

Equation (4) can be expressed as

$$Y = K_0 + B_0 X \quad (6)$$

where $Y = \frac{NRT\delta}{\Delta PM\overline{\nu}}$ and $X = \frac{P_{avg}}{\mu\overline{\nu}}$. So, K_0 and B_0 can be obtained from experimental data by plotting Y vs. X.

The mean porous radius can be calculated from Eqs. (3) and (4) as

$$r = \frac{16B_0}{3K_0}$$

and ε/τ can be obtained from Eq. (4)

The mean free path of CO_2 at P = 1 atm and T = 293 K is estimated to be about 0.087 μm. As this value is smaller than the pore size of the porous structure observed by SEM in our membranes and as the pressure was intermediate, the DGM was used to obtain pore sizes from gas permeation experiments. This model has already been used to determine mass transport characteristics of polyethylene and polypropylene porous membranes from CO_2 permeation determinations (29,30).

RESULTS AND DISCUSSION

The cross sections of the HF are shown in Fig. 3 while Fig. 4 presents a typical view of the external surface of the HF obtained with different dope solution. As expected, the internal coagulant and the air gap had an important effect on membrane structure.

When water was used as the bore liquid or coagulation bath (HF from series 1), finger like pores were observed in the inner part of the HF. In 1a, (air gap = 0.6 cm) finger like pores can be observed in the outer part due to the quick immersion of the nascent fiber into water.

As the air gap increased, air moisture diffusion through the fiber wall produced phase inversion at a lower rate than in the case of liquid water, leading to a sponge-like structure with small macrovoids in the outer part of the membrane. The use of water as the bore liquid together with air gaps larger than 0.6 cm led to a superposition of both external sponge-like and internal finger-like structures. This superposition was the result of two phase-inversion processes occurring at different rates. HF 1a shows a square-shape deformation. However, an air gap increase stabilized the nascent fiber, eliminating this deformation.

Using NMP/water mixture as the bore liquid (HF set number 2) decreased water diffusion by decreasing water activity as both are directly related (31–33), producing a sponge-like structure with small macrovoids. Outer

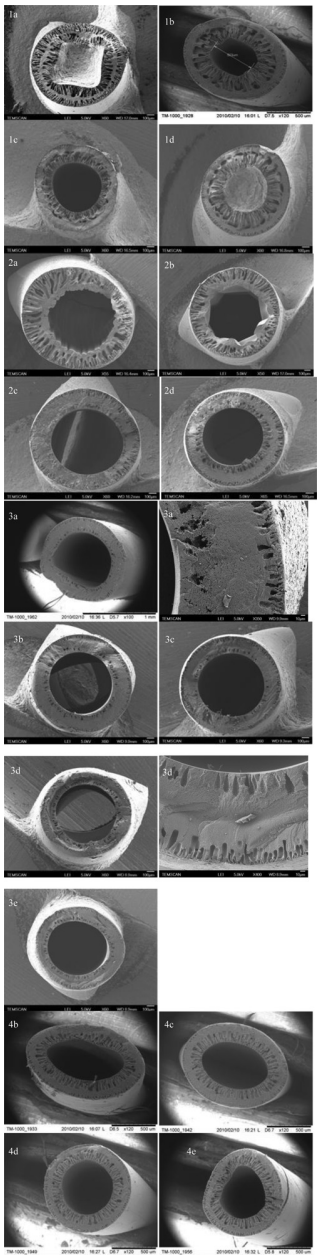

FIG. 3. Cross section of hollow fiber membranes obtained by varying the internal coagulant and the air gap. Internal coagulant 1: water, 2: Water/NMP (50%, 50%), 3: Water/NMP/PVA (46%, 46%, 8% respectively) 4: Water/PVA (92%, 8% respectively) (deformation in set 4 and in 3a is due to microscope holder and not to membrane fabrication). Letters a to e are associated to different air gaps described in Table 1.

structures presented large macrovoids (2a and 2b) as a result of immersion of the nascent fiber in water. These macrovoids tended to disappear with an air gap increase (2c, 2d) as a consequence of moisture diffusion. 2a and 2b HF inner shapes are deformed, whereas, in the other cases, the inner shapes were tubular which can be

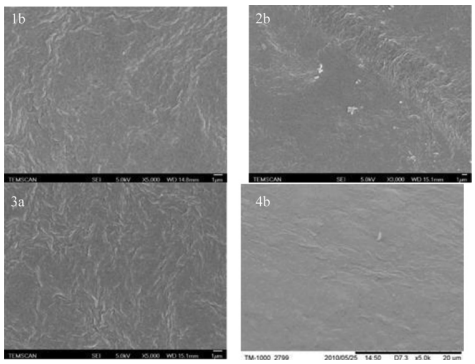

FIG. 4. Typical external surfaces of hollow fiber membranes obtained by varying the internal coagulant.

attributed to the die swell of PVDF macromolecules when exiting from the spinneret, this die swell is accentuated the air gap increase.

An NMP/Water/PVA mixture employed as the bore liquid (set number 3) led to a sponge like structure with small macrovoids both in the outer and the inner part of the HF structure. In all cases, no deformation of the inner shape was observed (the slight deformation observed in fiber 3a is due to microscope holder and not to membrane fabrication). Compared to the use of NMP/water mixture, the addition of PVA increased the viscosity and the osmotic pressure of the bore liquid and consequently decreased the activity of the solvents. Water and NMP diffusion through the inner surface decreased, retarding phase inversion phenomena. However, it is quite surprising that this effect also affected the phenomena at the outer surface of the dope solution: when the air gap was close to 0, no finger-like macrovoids were observed but a sponge-like structure with very small macrovoids was present. This was due to the diffusion of NMP through the wall of the fiber, leading to a decrease of the kinetics even at the outer surface.

The use of water/PVA solution led to a decrease of water activity due to the increase of the osmotic pressure. The osmotic pressure of this PVA solution is of the order of 50 kPa (34). From the osmotic pressure, it is possible to calculate the water activity a_1 using the equation:

$$\pi = -\frac{RT}{V_1}\ln(a_1)$$

where

R is the universal gas constant (8.314 J mol^{-1} K^{-1})

T is the absolute temperature (K)

V_1 is the water molar volume (m^3 mol^{-1})

Water activity in the case of water/PVA is close to 1 (0.996 for instance) whereas, in the Water/NMP solution, the water activity was far below 1 due to the high NMP concentration. Observations made on fibers numbered 1 and 4 showed the same kind of structure: a sponge-like structure with small macrovoids in the outer part of the fiber and large macrovoids in the inner part. Fibers produced with no air gap were deformed. Macrovoids of the inner part of the fiber were smaller in the case of water/PVA (length about 110 μm and width about 40 μm) than in the case of pure water (length about 300 μm and width about 100 μm).

Comparing fibers 3 and 4, the effect of NMP on water activity is clear: large macrovoids do not appear when NMP is present. We observe the same effect in the presence of PVA. In the case of PVA it has been shown by XPS and EDAX studies that when a water/PVA solution is used on PVDF membranes, poly(vinyl alcohol) adsorbs on the surface of the polymer changing its nature from hydrophobic to hydrophilic increasing its wettablity and hence its water affinity (35). In the case of NMP, an explanation can be given as follows: water has a higher chemical affinity for NMP than for PVA. From the point of view of molecular structure, oxygen is more electronegative than nitrogen; the partial positive charge of nitrogen and the negative charge of oxygen confer a strong electron acceptor donor character on the molecule of NMP, which can act as a hydrogen acceptor as well. This character allows NMP to form hydrogen bonds with the hydroxyl groups from PVA. On the other hand, the hydroxyl groups of water are much weaker sites for forming hydrogen bonds with PVA (36–38). So NMP works as a bridge between PVA and water, decreasing water activity and increasing that of PVA. Kim et al. (38) have observed that increasing NMP concentration in a PVA/NMP/water system in PVA membrane formation induces a phase transition by decreasing the solvation power of water for PVA. This yields more porous structures (sponge-like structures) with a dense skin. Hong et al. (37) have proposed that the dynamic behavior of PVA/NMP diluted solutions are driven by thermodynamic forces, in contrast to the situation in solutions of PVA/water, where hydrodynamic forces drive the dynamic behavior. It can thus be concluded that, in order to decrease the water activity sufficiently and control the phase inversion to obtain a sponge-like structure, NMP needs to be added to our system, together with PVA.

Viscosity of the internal coagulant, air gap, and decrease of water activity had a major effect on wall thickness. In general, an increase in bore liquid viscosity and air-gap forced the wall thickness to decrease and favored a sponge-like structure free of macrovoids as a result of liquid-liquid demixing against solid-liquid demixing (38b). HFs obtained with water/NMP/PVA solution had the narrowest walls, as a sponge-like structure is more compact than one with finger-like pores or a superposition of the two. This was true for air gaps greater than 20 cm. In the case of water and water/NMP bore solutions, when an air-gap

smaller than 20 cm was used, a strong deformation of the nascent fiber was observed. A similar phenomenon was observed by Bonyadi et al. (18) in the preparation of PVDF by phase inversion at air gaps smaller than 20 cm, due to instabilities created by a combination of hydrodynamics, mass transfer, convective flow and phase-separation processes (39–41).

Figure 5 shows typical surfaces observed in three different cases (sets 1, 2 and 3). As PVDF is a semi-crystalline polymer, liquid-liquid demixing is present during phase inversion, together with solid-liquid demixing (42). The structures obtained on the surfaces of our membranes are typical of solid-liquid demixing during inversion of phases as has been reported in previous studies (43,44) (leafy structure (15)). When the coagulation bath temperature is low (25°C), solid-liquid demixing starts quickly and dominates the precipitation process against the liquid-liquid demixing process, which is favored at higher temperatures (44). Cellular pores derived typically from a liquid-liquid demixing process are not present at the surfaces of our membranes (43).

Water Permeability

Pure water wet permeability values are reported in Table 1, with the geometrical dimensions of the HF, CO_2 permeability, and compaction pressures. As expected, pure water permeability decreased with water activity in the internal coagulant excepting the case of water/PVA. As previously pointed out, the use of water as the bore liquid led to a sponge-like structure together with finger-like pores and superficial pores giving high water permeability (131–77 $Lh^{-1}m^{-2}bar^{-1}$). When water/NMP/PVA was used, water activity decreased, giving internal and external surfaces with few or no pores at all as a result of PVDF solid-liquid demixing (fiber 3a in Fig. 3) leding to a dramatic decrease in water permeability to 5 $Lh^{-1}m^{-2}bar^{-1}$. Lastly, when the mixture of water/NMP and water/PVA was employed, intermediate water permeability was obtained as a result of an intermediate decrease in water activity. In the case of water/PVA used as internal liquid, adsorption of PVA on the surface of the polymer modifies its nature from hydrophobic to hydrophilic increasing its wettability and hence its water affinity (35) resulting in an increment of water diffusion.

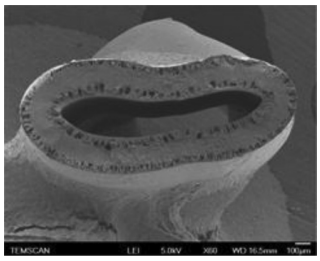

FIG. 5. Fiber 3a after compaction at 8 bars.

Concerning the air gap, for series 1 and 2, the permeability decreased when the air gap increased. Remarkably, when only PVA was added to the bore fluid (series 3) water permeability did not change with the air gap, except for the highest air gap, meaning that permeability was controlled by the decrease in water activity when PVA and NMP were used together.

CO_2 Permeability

CO_2 permeability followed the same trend as water permeability. It showed a decrease when PVA was added to the bore solution. When water or water/NMP was used, CO_2 permeability did not change, showing that the addition of PVA was responsible for this decrease. Again, adding NMP together with PVA to the bore solution decreased CO_2 permeability. For the first two sets of HF, permeability was in good agreement with values reported previously in the literature (11). When PVA was used, a considerable decrease in CO_2 permeability was observed. Nevertheless, these low permeability values are comparable to those of Polysulfone and other commercial membranes (45).

Water and CO_2 compaction tests allowed the evolution of mechanical resistance with water activity to be studied. Mechanical resistance was inversely correlated to water permeability values: high water permeability values (sets number 1, 2a, 3d, 4c, 4d) were found in membranes with low compaction resistance (membranes with finger-like pores). Conversely, more resistant membranes presented lower water permeability values (membrane 2d and set number 3), which were the membranes with predominantly sponge-like structure and internal and external skins. Concerning CO_2 compaction pressure, the most resistant membranes were obtained with water/PVA as the bore liquid. These tests agree well with the mechanical resistances shown in Table 3. As can be observed in this table, lower rigidity in the membrane (series 1, elongations at rupture close to 200%) was observed for membranes with lower CO_2 compaction pressures (3–5 $NLh^{-1}m^{-2}bar^{-1}$) and, when high rigidities were present (series 4, 57–79% of elongation at rupture), CO_2 compaction pressure was high (5–17 bar). Figure 5 shows that, after compaction, the global structure remained unchanged. Compacted membrane does not show any sign of swelling provoked by CO_2.

Mechanical Resistance

Table 3 shows the mechanical resistance results.

A great difference in membrane elasticity was observed between the set of membranes fabricated with PVA and those fabricated without adding PVA to the bore solution. Adding PVA led to a material more resistant to deformation (lower elongation at rupture), as a result of the

TABLE 3
Mechanical resistance of the hollow fibers prepared

Membrane	Tensile strength at break (N/mm^2)	Elongation at break (%)	Tensile strength at the elastic limit (N/mm^2)	Elongation at the elastic limit (%)
1a	36.6	235.2	13.8	13.5
1b	2.3	122.4	1.7	8.9
1c	54.3	213.8	17.8	8.4
1d	2.4	188.3	5.6	31.6
2a	2.2	96.7	1.8	27.9
2b	3.0	129.0	1.9	13.8
2c	3.3	119.0	2.0	12.3
2d	3.4	165.0	2.1	17.3
3a	5.6	45.3	3.2	3.5
3b	9.8	69.8	17.6	10.2
3c	41.4	94.6	19.0	2.1
3d	45.5	91.7	20.8	5.3
3e	32.6	84.7	18.4	5.5
4b	3.6	57.8	2.3	4.2
4c	3.5	69.9	2.2	3.8
4d	3.9	78.9	2.5	3.8
4e	3.1	74.4	2.0	3.9

sponge-like structure. The membranes most resistant to breaking obtained with water/NMP/PVA as the internal fluid, undoubtedly because the sponge-like structure was more accentuated in this set of membranes.

Pore Size Determination by the "Dusty Gas" Model

DGM allowed theoretical calculations of pore size for samples 3a and 3d and the set of membranes obtained with water/NMP as the bore liquid. Table 4 shows the results of these calculations.

TABLE 4
Geometrical parameters obtained from DGM for membranes with different internal coagulants

Membrane	K_0 (m) (10^{-9})	B_0 (m^2) (10^{-15})	r (μm)	ε/τ (10^{-2})
1c	8.97	4.98	2.9	0.45
2a	7.7	4.8	3.3	0.35
2b	5.4	4.3	4.2	0.19
2c	11	9.0	4.4	0.37
2d	4.3	1.5	1.9	0.34
3a	0.069	0.034	2.6	0.004
3b	0.006	3000	2.5	0.0003
3c	0.03	0.061	10.8	0.0004
4c	1.13	0.0135	0.6	0.26
4d	0.07	0.0035	2.6	0.004
4e	0.29	0.13	2.4	0.018

As can be observed, DGM predicted small pore sizes for all the membranes where it was tested (0.6 to 10.8 μm). These sizes agree well with a sponge-like structure but not with the finger-like pores observed in set number 2 or the small microvoids observed in 3a and 3d membranes. These differences arise from the restrictions imposed on DGM during the solving of the transport equations: low velocity flow, absence of turbulence (very low Reynolds numbers), and one-dimensional approach. What is most important is that the DGM was developed by treating the porous medium as one component of the gas mixture, consisting of giant molecules fixed in space, and the highly developed kinetic theory of gases was applied to this super-mixture (22). This treatment of the porous media as aggregates of spherical particles is more convenient for a sponge-like structure than for almost-cylindrical finger-like pores (better described by Poiseuille flow treatments). Nevertheless, the simplified model proposed by Izquierdo (26) and used in this study takes cylindrical pores into account for K_0 and B_0 calculation. Another source of differences between the model and the actual material is that the morphological parameters B_0 and K_0 represent average values across the medium, which is incorrect as the membranes show a gradual change in morphology. These kinds of membranes could be better modeled as two-layered structures, taking changes in K_0 and B_0 into account. However, a treatment like this is beyond the scope of this study. On the other hand, the porosity-tortuosiy factors obtained (ε/τ) agree well with a sponge-like structure such as the one

we obtained, as large values of τ represent highly interconnected pores, efficient in percolation paths. The values obtained for ε/τ agree well with the results obtained for permeability: the membranes with high permeability (1c, water 78 $Lh^{-1}m^{-2}bar^{-1}$, CO_2 53200 $NLh^{-1}m^{-2}bar^{-1}$) presented a high ε/τ value (0.45×10^{-2}) while membranes from set number 3 (permeability: water 4–5 $Lh^{-1}m^{-2}$ bar^{-1}, CO_2 720–1200 $NLh^{-1}m^{-2}bar^{-1}$) presented ε/τ values between 4×10^{-6} and 4×10^{-5}, in good agreement with the structure of these membranes, closer to a complete sponge-like structure where high water and/or gas fluxes across the structure mean that these fluids can circulate freely through the structure to find an exit in a system where no or few surface pores are present. This freedom is represented by low ε/τ values.

CONCLUSIONS

Four different internal coagulants were used to fabricate PVDF hollow fibers in order to study the role of viscosity in the structure of the membrane obtained. Higher viscosity resulted in a better structure, closer to the sponge-like structure. The air gap was optimized to obtain fewer and/or smaller macrovoids. We have demonstrated that an aqueous solution of PVA together with NMP as bore solution is needed to delay the activity of the water sufficiently to obtain resistant sponge-like structures. These membranes presented a collapse pressure of 8 bars due to the sponge-like structure developed. When PVA or NMP alone was used with water, the decrease in activity was not sufficient and finger-like pores were obtained. The air-gap has a marked effect on outer surface morphologies as a result of a controlled phase inversion induced by air moisture before immersion in the coagulation bath. This phenomenon allowed the morphology to be controlled by adjusting the air-gap. CO_2 permeability values were found to agree with values reported in the literature for PVDF membranes.

CO_2 permeability measurements allowed the "Dusty Gas Model" to be applied, which permitted the pore sizes and porosity-to-tortuosity factor to be determined. These calculations gave results close to the observations by SEM regarding the sponge-like structure. However, when this model was applied to an asymmetric membrane, finger-like pores were not accurately modeled. Modeling of the asymmetric membranes as two-layered structures is envisaged.

This study is a step forward in the understanding and control of PVDF membrane morphology and should contribute to the effort to produce suitable membranes for greenhouse gas capture.

ACKNOWLEDGEMENTS

The authors thank the French National Agency for Research for funding this study through the CICADI project ANR-06-CO2-002.

REFERENCES

1. (a) de Montigny, D.; Tontiwachwuthikul, P.; Chakma, A. (2005) Comparing the absorption performance of packed columns and membrane contactors. *Industrial & Engineering Chemistry Research*, 44 (15): 5726–5732; (b) Feron, P.H.M.; Jansen, A.E. (2002) CO_2 separation with polyolefin membrane contactors and dedicated absorption liquids: Performances and prospects. *Sep. Purif. Technol.*, (27): 231–242.
2. Ho, M.T.; Allinson, G.W.; Wiley, D.E. (2008) Reducing the cost of CO_2 capture from flue gases using membrane technology. *Industrial & Engineering Chemistry Research*, 47 (5): 1562–1568.
3. Ebner, A.D.; Ritter, J.A. (2009) State-of-the-art adsorption and membrane separation processes for carbon dioxide production from carbon dioxide emitting industries. *Separation Science and Technology*, 44 (6): 1273–1421.
4. Favre, E. (2007) Carbon dioxide recovery from post-combustion processes: Can gas permeation membranes compete with absorption? *Journal of Membrane Science*, 294 (1–2): 50–59.
5. http://www.liquicel.com/
6. Kosaraju, P.; Kovvali, A.S.; Korikov, A.; Sirkar, K.K. (2004) Hollow fiber membrane contactor based CO_2 absorption & stripping using novel solvents and membranes. *Industrial & Engineering Chemistry Research*, 44 (5): 1250–1258.
7. Mansourizadeh, A.; Ismail, A.F.; Matsuura, T. (2010) Effect of operating conditions on the physical and chemical CO_2 absorption through the PVDF hollow fiber membrane contactor. *Journal of Membrane Science*, 353 (1–2): 192–200.
8. Akira Kaito, Y.L.; Masaki, Shimomura; Shuichi, Nojima. (2009) Oriented lamellar structures in uniaxially drawn films of poly(vinylidene fluoride) and poly(3-hydroxybutyrate) blends studied by small-angle X-ray scattering measurements. *Journal of Polymer Science Part B: Polymer Physics*, 47 (4): 381–392.
9. Yakai Lin, Y.T.; Hengyu, Ma; Jian, Yang; Ye, Tian; Wenzhong, Ma; Xiaolin, Wang. (2009) Formation of a bicontinuous structure membrane of polyvinylidene fluoride in diphenyl carbonate diluent via thermally induced phase separation. *Journal of Applied Polymer Science*, 114 (3): 1523–1528.
10. Cheng, T.-W.; Han, C.-J.; Hwang, K.-J.; Ho, C.-D.; Cooper, W.J. (2010) Influence of feed composition on distillate flux and membrane fouling in direct contact membrane distillation. *Separation Science and Technology*, 45 (7): 967–974.
11. Mansourizadeh, A.; Ismail, A.F.; Abdullah, M.S.; Ng, B.C. (2010) Preparation of polyvinylidene fluoride hollow fiber membranes for CO_2 absorption using phase-inversion promoter additives. *Journal of Membrane Science*, 355 (1–2): 200–207.
12. Rezakazemi, M.; Niazi, Z.; Mirfendereski, M.; Shirazian, S.; Mohammadi, T.; Pak, A. (2011) CFD simulation of natural gas sweetening in a gas, Äliquid hollow-fiber membrane contactor. *Chemical Engineering Journal*, 168 (3): 1217–1226.
13. Atchariyawut, S.; Feng, C.; Wang, R.; Jiraratananon, R.; Liang, D.T. (2006) Effect of membrane structure on mass-transfer in the membrane gas-liquid contacting process using microporous PVDF hollow fibers. *Journal of Membrane Science*, 285 (1–2): 272–281.
14. Xu, A.; Yang, A.; Young, S.; deMontigny, D.; Tontiwachwuthikul, P. (2008) Effect of internal coagulant on effectiveness of polyvinylidene fluoride membrane for carbon dioxide separation and absorption. *Journal of Membrane Science*, 311 (1–2): 153–158.
15. Reverchon, E.; Cardea, S. (2006) PVDF-HFP membrane formation by supercritical CO_2 processing: Elucidation of formation mechanisms. *Industrial & Engineering Chemistry Research*, 45 (26): 8939–8945.
16. Morehouse, J.A.; Taylor, D.L.; Lloyd, D.R.; Lawler, D.F.; Freeman, B.D.; Worrel, L.S. (2006) The effect of uni-axial stretching on the roughness of microfiltration membranes. *Journal of Membrane Science*, 280 (1–2): 712–719.

17. Morehouse, J.; Worrel, L.; Taylor, D.; Lloyd, D.; Freeman, B.; Lawler, D. (2006) The effect of uni-axial orientation on macroporous membrane structure. *Journal of Porous Materials*, 13 (1): 61–72.
18. Bonyadi, S.; Chung, T.S.; Krantz, W.B. (2007) Investigation of corrugation phenomenon in the inner contour of hollow fibers during the non-solvent induced phase-separation process. *Journal of Membrane Science*, 299 (1–2): 200–210.
19. Lei, C.; Wang, Q.; Li, L. (2009) Effect of interactions between poly(vinyl alcohol) and urea on the water solubility of poly(vinyl alcohol). *Journal of Applied Polymer Science*, 114 (1): 517–523.
20. Shenoy, S.L.; Fujiwara, T.; Wynne, K.J. (2003) Quantifying plasticization and melting behavior of poly(vinylidene fluoride) in supercritical CO_2 utilizing a linear variable differential transformer. *Macromolecules*, 36 (9): 3380–3385.
21. Mason, E.A.; Malinauskas, A.P.; Evans, R.B. (1967) Flow and diffusion of gases in porous media. *Journal of Chemical Physics*, 46: 3199–4.
22. Mason, E.A.; Malinuskas, A.P. (1983) *Gas Transport in Porous Media: The Dusty-Gas Model*; Elsevier: Amsterdam.
23. Babu, B.R.; Rastogi, N.K.; Raghavarao, K.S.M.S. (2006) Mass transfer in osmotic membrane distillation of phycocyanin colorant and sweet-lime juice. *Journal of Membrane Science*, 272 (1–2): 58–69.
24. Srisurichan, S.; Jiraratananon, R.; Fane, A.G. (2006) Mass transfer mechanisms and transport resistances in direct contact membrane distillation process. *Journal of Membrane Science*, 277 (1–2): 186–194.
25. Fernández-Pineda, C.; Izquierdo-Gil, M.A.; García-Payo, M.C. (2002) Gas permeation and direct contact membrane distillation experiments and their analysis using different models. *Journal of Membrane Science*, 198 (1): 33–49.
26. Izquierdo-Gil, M.A. (2008) Temperature influence on transport parameters characteristic of Knudsen and Poiseuille flows. *Chemical Engineering Science*, 63 (22): 5531–5539.
27. Chakrabarty, B.; Ghoshal, A.K.; Purkait, M.K. (2008) SEM analysis and gas permeability test to characterize polysulfone membrane prepared with polyethylene glycol as additive. *Journal of Colloid and Interface Science*, 320 (1): 245–253.
28. Lawson, K.W.; Hall, M.S.; Lloyd, D.R. (1995) Compaction of microporous membranes used in membrane distillation. I. Effect on gas permeability. *Journal of Membrane Science*, 101 (1–2): 99–108.
29. Guijt, C.M.; Rácz, I.G.; Reith, T.; de Haan, A.B. (2000) Determination of membrane properties for use in the modelling of a membrane distillation module. *Desalination*, 132 (1–3): 255–261.
30. Guijt, C.M.; Meindersma, G.W.; Reith, T.; de Haan, A.B. (2002) Method for experimental determination of the gas transport properties of highly porous fibre membranes: A first step before predictive modelling of a membrane distillation process. *Desalination*, 147 (1–3): 127–132.
31. Majsztrik, P.W.; Satterfield, M.B.; Bocarsly, A.B.; Benziger, J.B. (2007) Water sorption, desorption and transport in Nafion membranes. *Journal of Membrane Science*, 301 (1–2): 93–106.
32. Majsztrik, P.; Bocarsly, A.; Benziger, J. (2008) Water permeation through Nafion membranes: The role of water activity. *The Journal of Physical Chemistry B*, 112 (51): 16280–16289.
33. Zhao, Q.; Majsztrik, P.; Benziger, J. (2011) Diffusion and interfacial transport of water in Nafion. *The Journal of Physical Chemistry B*, 115 (12): 2717–2727.
34. Horkay, F.; Hecht, A.-M.; Geissler, E. (1998) Fine structure of polymer networks as revealed by solvent swelling. *Macromolecules*, 31 (25): 8851–8856.
35. Gholap, S.G.; Badiger, M.V.; Gopinath, C.S. (2005) Molecular origins of wettability of hydrophobic poly(vinylidene fluoride) microporous membranes on poly(vinyl alcohol) adsorption: Surface and interface analysis by XPS. *The Journal of Physical Chemistry B*, 109 (29): 13941–13947.
36. Po-Da Hong, H.-T.H., (2000) Effect of co-solvent complex on preferential adsorption phenomenon in polyvinyl alcohol ternary solutions. *Polymer*, 41: 6195–4.
37. Po-Da Hong, C.-M.C.; Chiu-Hui, He. (2001) Solvent effects on aggregation behavior of polyvinyl alcohol solutions. *Polymer*, 42: 6105–4.
38. (a) Sang-Gyun Kim, Y.-I.K.; Hyung-Gu, Yun.; Gyun-Taek, Lim.; Kew-Ho, Lee. (2003) Preparation of asymmetric PVA membranes using ternary system composed of polymer and cosolvent. *J. Appl. Polym. Sci.*, 88: 2884–4; (b) Panu, Sukitpaneenit; Tai-Shung, Chung. (2011) Molecular design of the morphology and pore size of PVDF hollow fiber membranes for ethanol–water separation employing the modified pore-flow concept. *Journal of Membrane Science*, 374: 67–82.
39. Barrande, M.; Bouchet, R.; Denoyel, R. (2007) Tortuosity of porous particles. *Analytical Chemistry*, 79 (23): 9115–9121.
40. Guijt, C.M.; Meindersma, G.W.; Reith, T.; de Haan, A.B. (2005) Air gap membrane distillation: 1. Modelling and mass transport properties for hollow fibre membranes. *Separation and Purification Technology*, 43 (3): 233–244.
41. Guijt, C.M.; Meindersma, G.W.; Reith, T.; Haan, A.B.D. (2005) Air gap membrane distillation: 2. Model validation and hollow fibre module performance analysis. *Separation and Purification Technology*, 43 (3): 245–255.
42. Panu Sukitpaneenit, T.-S.C., (2009) Molecular elucidation of morphology and mechanical properties of PVDF hollow fiber membranes from aspects of phase inversion, crystallization and rheology. *J. Membr. Sci.*, 340: 192–4.
43. Lin, D.-J.; Chang, C.-L.; Huang, F.-M.; Cheng, L.-P., (2003) Effect of salt additive on the formation of microporous poly(vinylidene fluoride) membranes by phase inversion from LiClO4/Water/DMF/PVDF system. *Polymer*, 44 (2): 413–422.
44. Cheng, L.-P., (1999) Effect of temperature on the formation of microporous PVDF membranes by precipitation from 1-octanol/DMF/PVDF and water/DMF/PVDF systems. *Macromolecules*, 32 (20): 6668–6674.
45. Lara-Estévez, J.C.I.; Camacho-Zuñiga, C.; Ruiz-Treviño, F.A.; Bucio, E.; Cassidy, P.E.; Booth, C.J. (2010) Gas transport properties of some fluorine-containing polyethers. *Industrial & Engineering Chemistry Research*, doi: 10.1021/ie100249j.